Weather and Climate Extremes 13 (2016) 1–14

Contents lists available at ScienceDirect

Weather and Climate Extremes

journal homepage: www.elsevier.com/locate/wace

Long-term variability of the leading seasonal modes of rainfall in south-eastern Australia

Maryam Montazerolghaem *, Willem Vervoort, Budiman Minasny, Alex McBratney

Faculty of Agriculture and Environment, The University of Sydney, Sydney, Australia

ARTICLE INFO

Article history:
Received 13 July 2015
Received in revised form
14 April 2016
Accepted 17 April 2016
Available online 4 May 2016

Keywords:
Climate variability
Seasonal rainfall
Sptio-temporal analysis
Australian climate drivers
PCA analysis
Running correlation

ABSTRACT

Knowledge of temporal and spatial variability of climate and rainfall can improve agriculture production and can help to manage risks caused by climate variability. Available high-quality monthly rainfall data from the Australian Bureau of Meteorology for 1907–2011 was used to investigate the leading seasonal mode of the long-term rainfall variability over south-eastern and eastern Australia. Spatio-temporal variations of seasonal rainfall and their connection to oceanic-atmospheric predictors were analysed. The links between the first two Principal Components of rainfall of each season with lagged Southern Oscillation Index (SOI), Indian Ocean Dipole (IOD) and Southern Annular Mode (SAM) were season-dependent. The relationship between these climatic indices changed within both inter-seasonal and decadal time scales. Spring and winter rainfalls were continuously positively correlated with lagged (SOI). However, summer rainfall variations indicated negative correlations with lagged SOI which increase from 1970. The correlations between lagged SOI and autumn variations were weak and change to a stronger relationship from 1990. Correlations between lagged (IOD) which varied across all seasons have recently been increasing. Variations in rainfall across all seasons were highly correlated with Southern Annular Mode (SAM) with different signs. Overall, the relationship between predictors and seasonal rainfall has changed after 1970. The results of running correlations between leading modes of seasonal rainfall and lagged SOI, SAM, and IOD indices indicates non-stationary in these links. The relationships of climatic indices and leading modes of seasonal rainfall changed since 1970, with stronger evidence in case of IOD. Recent changes in the relationships between climatic indices and rainfall need to be considered in climate prediction systems. The results of this study suggests that improvement in statistical regional rainfall forecast system with fixed climatic indices for each season and region is achievable by using suitable seasonal and regional climatic indices.

1. Introduction

Agricultural production and the population of Australia are both concentrated in the south-eastern part of the country. Rainfall over south-eastern Australia, and indeed over most of the continent, is highly variable spatially and across time scales ranging from daily to decadal. Rainfall and temperature regimes have a significant impact on agriculture decision points both in time and space (Nelson et al., 2010). Fine resolution climate information can be incorporated into farm business decisions and help to manage climate related risks (Hammer et al., 2001).

Seasonal rainfall patterns over Australia and related atmospheric circulation have been the topic of many studies (Drosdowsky and Chambers, 2001; Kirono et al., 2010; Murphy and Timbal, 2008; Nicholls, 2010; Risbey et al., 2009; Wang and Hendon, 2007). The link between rainfall variability of eastern and south-eastern Australia and oceanic atmospheric variations is highly seasonal and regional specific (Drosdowsky and Chambers, 2001; Evans et al., 2009; Kirono et al., 2010; Murphy and Timbal, 2008; Schepen et al., 2012). In particular, the El Niño–Southern Oscillation (ENSO) is indicated as the major driver of inter annual and decadal climate variability of Australia (Evans and Allan, 1992; Kirono et al., 2010; Robertson et al., 2013; Wang and Hendon, 2007). Temperatures in the tropical Indian Ocean also have an influence on eastern and south-eastern Australia's rainfall, particularly for winter rainfall (Cai et al., 2009; Nicholls, 1989; Verdon and Franks, 2005b; Verdon and Franks, 2006). The Indian Ocean Dipole (IOD) was found to be particularly important in the June-October period, which spans the wet seasons (spring-winter) over south-eastern Australia (Ashok et al., 2003; Risbey et al., 2009). The Southern Annular mode (SAM) (Hendon et al., 2007) is further considered as an extratropical source of variability that is mostly

* Corresponding author.
E-mail addresses: maryam.montazerolghaem@sydney.edu.au (M. Montazerolghaem), willem.vervoort@sydney.edu.au (W. Vervoort), budiman.minasny@sydney.edu.au (B. Minasny), alex.mcbratney@sydney.edu.au (A. McBratney).

http://dx.doi.org/10.1016/j.wace.2016.04.001

confined to the southwest and southeast of the continent (Risbey et al., 2009). The Madden–Julian Oscillation (MJO) (Wheeler and Hendon, 2004; Wheeler et al., 2009), which is linked to the ENSO, can influence rainfall in several areas of the continent in different seasons. The MJO's impact appears to be strongest in its effect on monsoon rains in the north of Australia (Risbey et al., 2009).

Different active times of Indian and Pacific Oceans, and interaction between ENSO and Indian Ocean events, result in complex relationships between these oceanic – atmospheric phenomena and Australian rainfall (Cai et al., 2013; Meyers et al., 2007). At decadal timescales, Australia and particularly its south-eastern regions have a high level of rainfall variability. The drivers for this are still not totally clear, although some of the variability is linked with variations in relative frequency of El Niño and La Niña events on decadal timescales. Interdecadal variability is particularly high across eastern Australia (Kiem and Franks, 2004; Kiem et al., 2003; Verdon et al., 2004).

Statistical seasonal forecast systems for Australia based on SSTs variations over the Pacific and Indian Oceans have been used at the Australian Bureau of Meteorology (Alves et al., 2003; Drosdowsky and Chambers, 2001; Stone et al., 1996). More recent Australian Bureau of Meteorology dynamical forecasts are determined by statistically calibrating rainfall from the Predictive Ocean Atmosphere Model (POAMA) (Hudson et al., 2011; Schepen et al., 2012). Using the strengths of the statistical and dynamical models is suggested to maximize the spatial and seasonal accuracy of seasonal rainfall forecasts (Schepen et al., 2012). The interaction between ENSO and Indian Ocean events, extreme events related mostly to the Indian Ocean events, and changes in the frequencies of IOD events were suggested to explain the recent unexpected changes in Australian rainfall and failed forecasts (Cai et al., 2009, 2013; Ummenhofer et al., 2009). However, further analysis is required to investigate the stability of the link between climate indices and seasonal rainfall variations of south-eastern and eastern Australia as predictors used in the Australian statistical seasonal rainfall forecast systems (Schepen et al., 2012; Drosdowsky and Chambers, 2001; Gergis et al., 2012; Kirono et al., 2010).

This study explores the temporal variability of the relationship between reasonable lags (up to six months) of climate indices and the main variations of seasonal rainfall across south-eastern and eastern Australia. Special emphasis is made on the seasonal differences in rainfall variability. The aims of this study are: 1) to provide an overall overview and summary of spatio-temporal seasonal rainfall variations from interannual to inter – decadal for south-eastern and eastern Australia; 2) to reconfirm the main mechanism of seasonal rainfall variations over southern and south-eastern Australia rainfall; 3) to check the stability of links between seasonal rainfall and different lags of major oceanic-atmospheric predictors (SAM, IOD and SOI) over more than 100 years data.

1.1. Data and area of study

The dataset in this study consists of 137 Australian Bureau of Meteorology (BoM) high-quality rainfall stations across south eastern and eastern Australia over 1879–2011 (Fig. 1) (Lavery et al., 1997). Seasons in this study are the standard calendar Australian seasons, defined as: December–January–February (DJF) for summer, March–April–May (MAM) for autumn, June–July–August (JJA) for winter, and September–October–November (SON) for spring. Missing data were dealt with following two rules: First, times with missing values at more than 30% of stations were omitted from the dataset. This resulted in the elimination of data before 1907. Secondly, the rest of missing values were replaced by the mean of the four closest stations in terms of geographical distance. This leads a

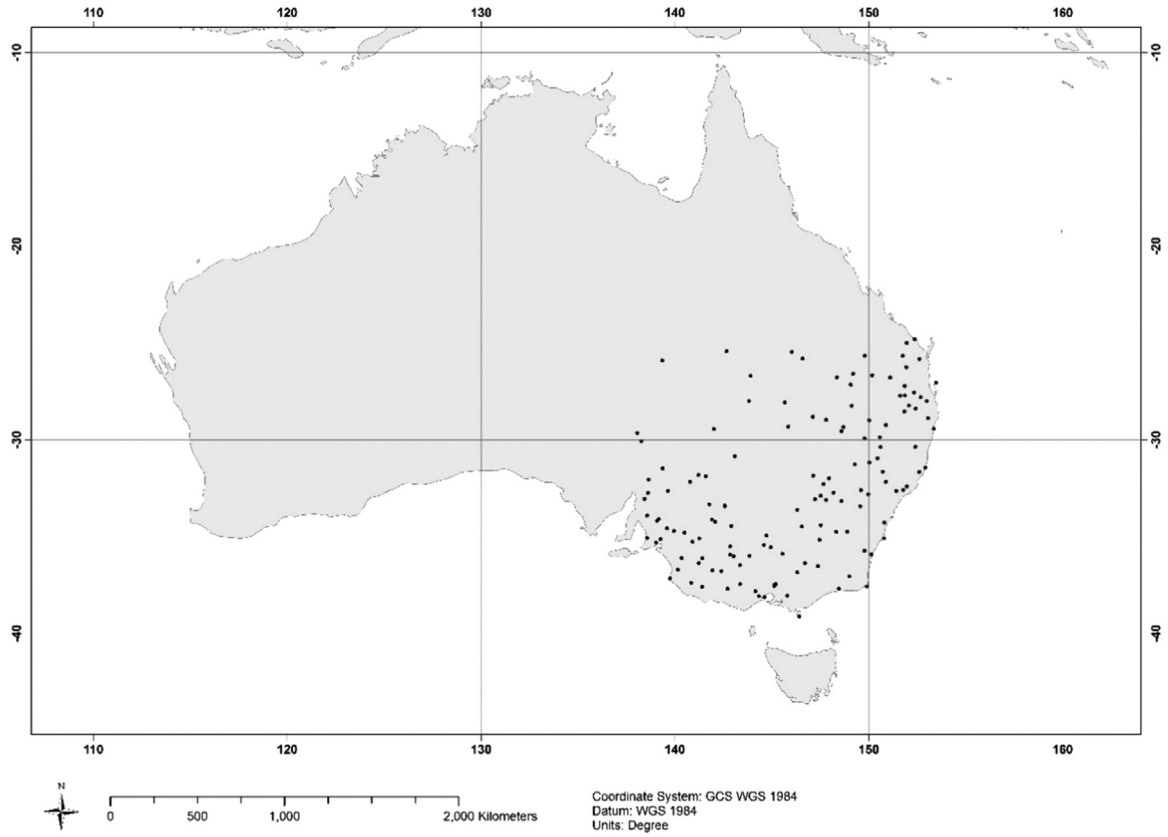

Fig. 1. Location map indicating high quality stations used in this study.

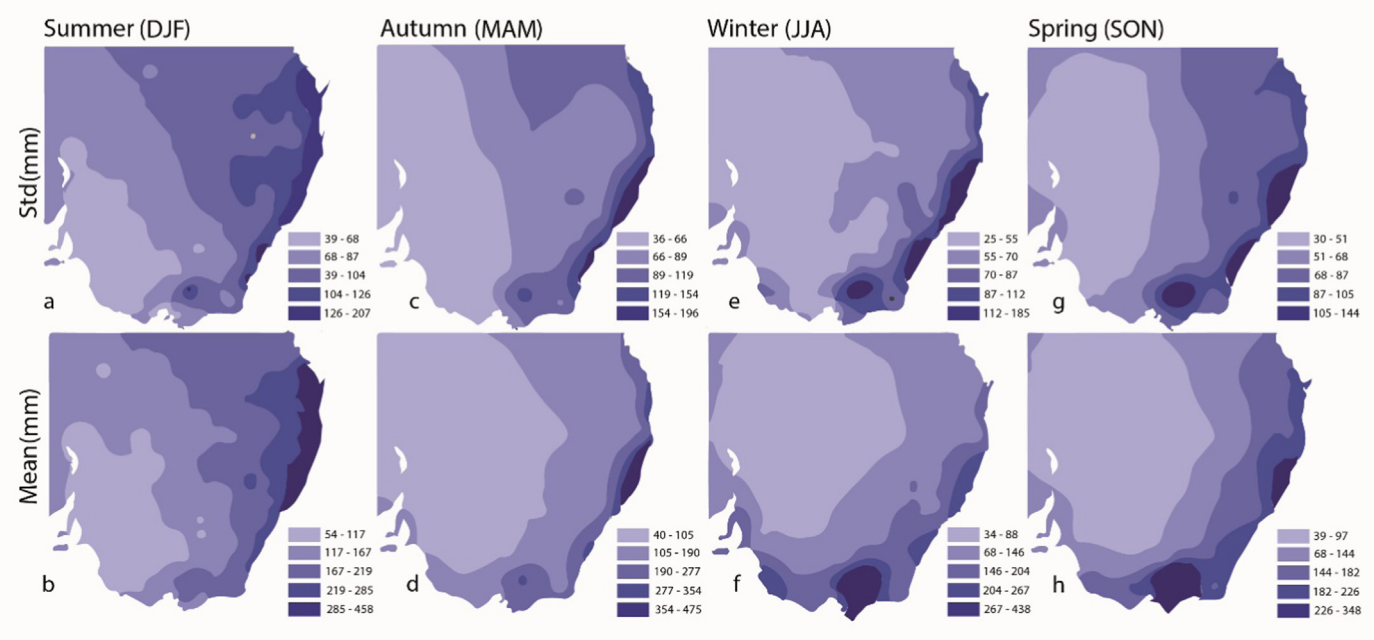

Fig. 2. Mean and standard deviation of seasonal rainfall for the period 1907–2011.

decreased time period to 1907–2011. Fig. 2 shows a map of long-term mean and standard deviation of seasonal rainfall in south-eastern Australia over 1907–2011.

Climatic indices used in this study are SOI, IOD and SAM, which have been highlighted as the main climate drivers of south-eastern and eastern Australia (Hendon et al., 2007; Kirono et al., 2010; Verdon and Franks, 2005a) (Table 1).

2. Methods

2.1. Spatial and temporal analysis using PCA

Extensive use has been made of Principal Component Analysis (PCA), correlation and regression methods to establish evidence of teleconnection between climatic indices and rainfall variation in Australia (Drosdowsky and Chambers, 2001; Drosdowsky, 2002; Kirono et al., 2010; Risbey et al., 2009).

There are two types of matrix structures that can be used for this type of analysis; the first one is (S-mode) analysis, which variables (columns) are stations, and observations (rows) are the values at each time point. In (S-mode) analysis, principal component coefficients, known as loadings, contain the correlation (coefficients) of each station with the corresponding PC. In the case of (S-mode), scores contain the time series of each component. This matrix structure ((S-mode)) is not recommended for spatial analysis and is suitable for temporal variation analysis. The second type is T-mode analysis where each individual time point is a variable (columns), and each station is an observation (rows). The result are components with loading on the individual time points, and amplitudes (scores) on the observation or spatial variables (Drosdowsky, 1993). This method is used mostly as pre-processing for clustering analysis in regionalization applications (Dezfuli, 2011; Richman, 1986). PCA provides a great interpretation opportunity since each component can be interpreted without reference to the others. The first PC accounts for the highest variation in the data, and tends to be a large scale average. The second PC tends to describe large scale contrasts mostly with dipoles loadings (Drosdowsky, 1993).

In this study (S-mode) PCA was used to analyse the spatial-temporal of the leading modes of the seasonal rainfall variability in the data. A running 20-year window correlation analysis was applied to investigate long-term stability and variations of the strength of links between atmospheric-oceanic predictors and seasonal rainfall in south-eastern Australia. The analysis was carried out using data from 1907 to 2011 for SOI and IOD and for SAM from 1957, because of available data for SAM.

Table 1
List of climatic indices and data sources used.

Climate indices	Definition	Period	Source
Southern Oscillation Index (SOI)	Normalized pressure difference between Tahiti and Darwin (Troup, 1965)	1876–2012	Bureau of meteorology http://www.bom.gov.au/climate/pi-cpp/download.shtml
Indian Ocean Dipole mode index (IODMI)	WPI–EPI (Saji et al., 1999)	1854–2008	NCAR, ERSST. v3 (Smith et al., 2008)
Southern Annular Mode (SAM)	MSLP difference between 40 s and 65 s	1957–2008	(Marshall, 2003)

3. Results and discussion

3.1. Leading modes of the seasonal mean rainfall ((S-mode) analysis)

Fig. 3 indicates the amount of variance explained by PCs of each season rainfall. In the results, only the first two PCs are considered, as each of the subsequent PCs explains less than 10% of the total rainfall variance in each season (Zveryaev, 2006).

Time series (standardised scores) and spatial patterns (loadings) of the first two PCs of rainfall are shown in Figs. 3 and 4. The loading plot is useful to identify spatial similarity. In Fig. 3, time series of the corresponding standardised anomalies of each season rainfall are given as a comparison to the scores plot of each PC. The standardised seasonal rainfall anomalies are the mean of the individual station anomalies; i.e., subtracting the station mean from the seasonal rainfall value and dividing by the standard deviation of the station data. Correlation between the first two PCs and corresponding season rainfall anomalies were calculated during

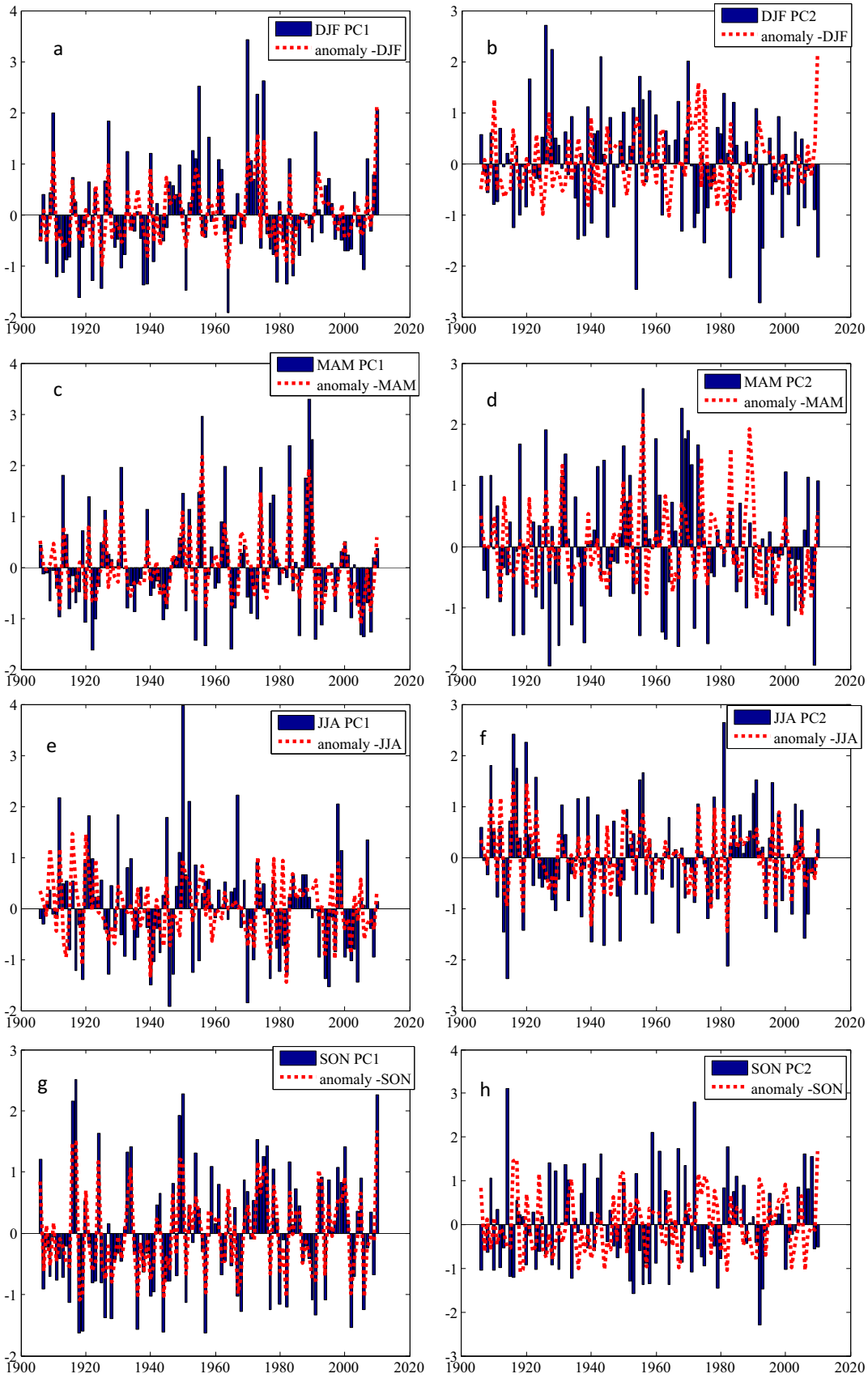

Fig. 3. Time series of standardised anomalies and normalized scores of the first two PCs of (a, b) summer (DJF), (c, d) autumn (MAM), (e, f) winter (JJA), and (g, h) spring (SON) rainfall (1907–2011).

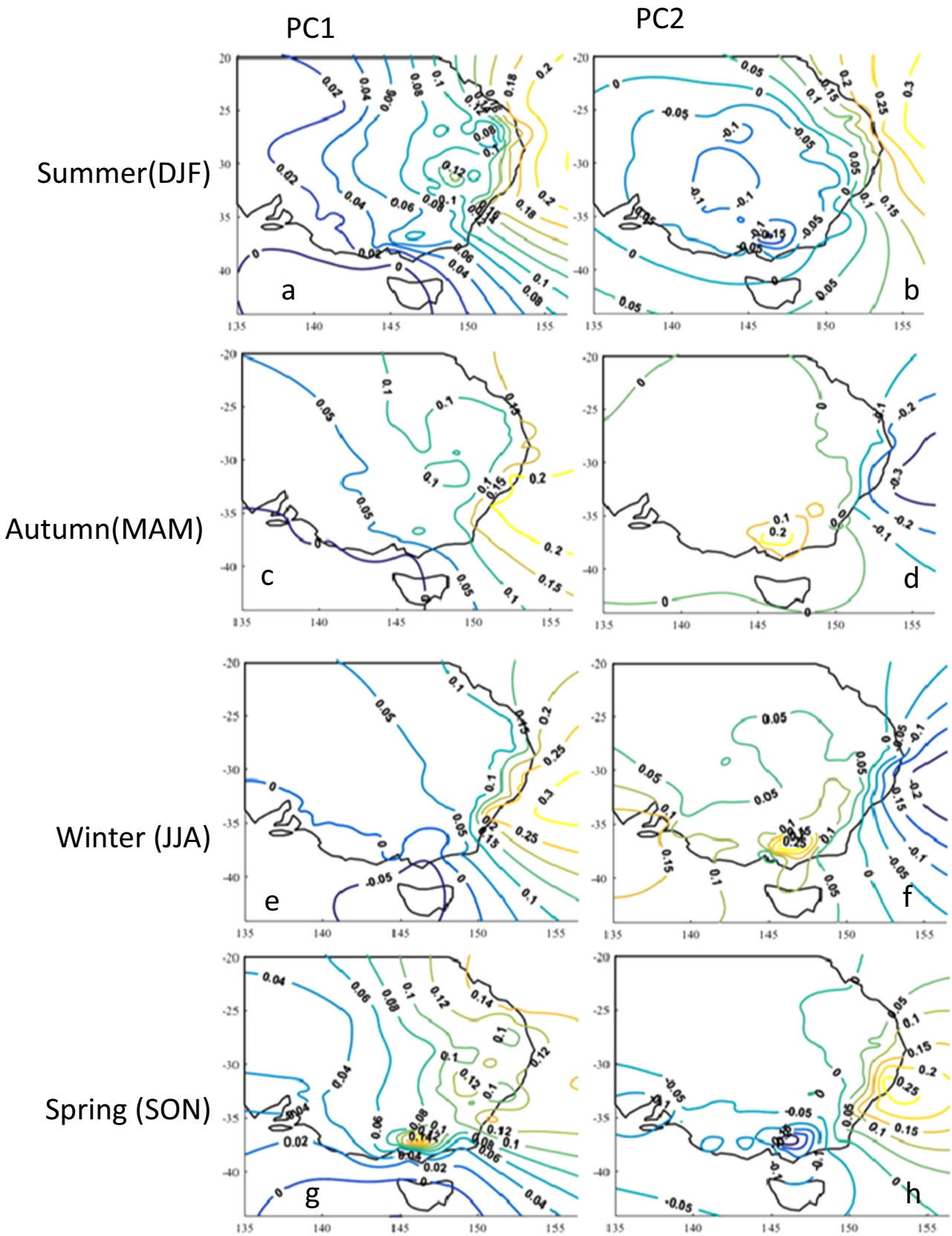

Fig. 4. Spatial pattern of the first two PCs of (a, b) summer, (c, d) autumn, (e, f) winter, and (g, h) spring rainfall over south-eastern Australia for period of 1907–2010.

different time periods (Table 2). The loading and score plot of the first two PCs of each season are explained separately.

The first principal component of summer ($PC1_{DJF}$) rainfall explains 36.96% of the total summer rainfall variance. The spatial pattern of PC1 has the same sign across the entire area, homogenous south-north and varies east-west with large positive

Table 2
Correlation between the first two PCs and corresponding season rainfall anomalies P-value = 0.05.

	Summer (DJF)	Autumn (MAM)	Winter (JJA)	Spring (SON)
PC1	0.86	0.9	0.53	0.96
PC2	−0.42	0.37	0.82	−0.267
PC1 (1907–1960)	0.85	0.9	0.5	0.96
PC2 (1907–1960)	−0.43	0.24	0.81	−0.1 (P-value = 0.4)
PC1 (1961–2011)	0.88	0.9	0.58	0.95
PC2 (1961–2011)	−0.49	0.5	0.84	−0.4

values in the eastern coastal area (Fig. 4a). The second PC of summer, $PC2_{DJF}$, explains 10.4% of the total variation of the summer rainfall. The respective spatial pattern reflects the summer rainfall and mean annual rainfall (Fig. 1b and Fig. 4b). The loadings of $PC2_{DJF}$ represent a dipole pattern with a negative value in the far western part of the study region, with a winter rainfall regime, and being positive in the eastern and northern part of the study region. Note that variables on opposite sides of the origin in the loading plot are negatively correlated. Therefore, the opposite loadings reflect the different rainfall regimes during summer across south-eastern Australia. The spatial pattern of the summer PC2 (Fig. 4b) is noticeably different from the PC2 during other seasons (Fig. 4d, f and h). Fig. 3b displays the temporal behaviour of the PC2 of summer rainfall featuring a downward trend from 1975 to recent. The scores of $PC1_{DJF}$ (Fig. 3a) indicate a long-term trend in comparison to the PC2, which includes shorter time variations. Note that the trend in the time series in Fig. 3 is the PC scores trend that can be different from the real rainfall time series trend. The trend in the real rainfall for each region is dependent on the sign of the loading, e.g. a positive trend in the score of individual year, may reflect both an increase and a decrease in rainfall in the area.

During autumn (MAM) the PC1 accounts for 36.9% of the rainfall variation. The respective spatial pattern (Fig. 4c) displays a similar pattern to mean annual rainfall pattern with decreasing loading west-east. The second PC explains 13.2% of the total variance of autumn precipitation. Spatial distributions of the second PC of autumn rainfall indicate positive loadings in the south and central parts of the study region, and negative loadings in the east and north of the region.

The trend in the autumn PC1 changed from an upward trend to a downward trend after 1990, when Australia experienced a significant drought (Fig. 3c). This PC displays long-term interdecadal variations. Similar to the summer PC2, the autumn PC2 (Fig. 3d) shows more year-to-year trends and is associated with short term variations.

During winter (JJA) $PC1_{JJA}$ represents 30.77% of the total rainfall variance. The respective spatial pattern is the only PC1 of seasonal rainfall that indicates negative loadings in the south, and reaches positive values in the coastal area in the east. The $PC2_{JJA}$ accounts for 24% of rainfall variance and explains the largest variation in rainfall compared to the PC2 of other seasons. The spatial pattern of the winter rainfall PC2 is very similar to the mean winter pattern (Figs. 1 and 4d). The spatial pattern of this PC is totally different from the spatial patterns PC2 of DJF and MAM (Fig. 4d).

In winter (JJA), the trend in the PC1 changes to downward after 1975 (Fig. 3e). In addition, the scores of the $PC1_{JJA}$ display long-term inter-decadal variations. The scores of $PC2_{JJA}$ show year-to-year trends and are associated with short term variations (Fig. 3f).

$PC1_{SON}$ accounts for 43.6% of the total variance of spring rainfall. Spring PC1 explains the largest amount of the seasonal rainfall compared to the PC1s of other seasons. The loading of spring PC1 is the same as the autumn and summer PC1 with positive loading over the entire area and a decrease in loading from west to east (Fig. 4g). The $PC2_{SON}$ accounts for 16.9% which is the second highest amount of explained seasonal variation after the winter PC2 (24.5%). As variables (stations) with opposite loading have strongly different patterns, PC2 represents seasonal behaviour of temperature variations or rainfall regime in the area. The PC1 of each season represents the annual rainfall pattern and mean annual rainfall in the area.

Summarizing results of this section, leading PCA modes of south-eastern Australia are clearly season-dependent. The PC1 of all seasons followed the seasonal rainfall anomalies (Fig. 3 and Table 2).

Spring and autumn rainfall PCs show higher correlation with annual rainfall PCs, followed by winter 0.7, 0.6 and 0.5 respectively. The correlation of annual rainfall with summer rainfall value of is not as strong as for other seasons. This suggests that the variance of annual rainfall is mostly dominated by the variance in the autumn and spring.

As seen in Table 3 the contribution of PCs to the seasonal rainfall variability changes during different decades. The contribution of the PC1 to summer rainfall variation changes from 32.7% in 1950–1970 to 52.2% in 1950–1970. In summer and autumn the amount of rainfall variation, which PC1 explained, has increased during recent decades. In comparison, the PC1 of winter and spring explains more of the rainfall variability over 1906–1950.

3.2. Running linear correlation between leading PCs with climatic indices

3.2.1. Summer

Running correlations for $PC1_{DJF}$ and $PC2_{DJF}$ versus three lags of SOI, IOD and SAM for up to six months are presented. For the analysis the average value of the last two months from the start of the season, Oct–Nov is used, denoted as SOI_{ON}, IOD_{ON} and SAM_{ON} (Fig. 5a and d). Similarly, the average of the last three and four months, Aug–Sep, is denoted as SOI_{AS}, IOD_{AS} and SAM_{AS} (Fig. 5b and e); and the average of the last five and six months, Jun–Jul, is denoted as SOI_{JJ}, IOD_{JJ} and SAM_{JJ} (Fig. 5c and f).

In summer, the results are four main fold; 1) all climate indices, SOI, IOD and SAM, are negatively correlated with summer rainfall anomalies; 2) from 1970, the strength of these relationships between summer rainfall and its predictors is getting stronger; 3) the most significant change occurred for the impact of IOD on summer rainfall; 4) the results show variable impact of the different lags of each predictors. For summer, PC1 and PC2, will be discussed separately.

Table 4 represents the correlation between the summer rainfall predictors with the same time lags used in the current study.

Table 3
Fraction of the total rainfall variances explained in each season by PC1 and PC2.

		Summer (DJF)	Autumn (MAM)	Winter (JJA)	Spring (SON)
PC1	1906–2010	36.96	36.9	30.77	43.6
	1906–1950	32.66	28.78	36.6	51.50
	1950–1970	52.17	45.17	35.41	42.25
	1970–2010	40.04	44.05	35.11	41.47
PC2	1906–2010	10.4	13.2	24.5	16.9
	1906–1950	12.21	15.1	27.49	15.47
	1950–1970	12.13	21.11	23.03	21.09
	1970–2010	11.59	10.15	21.08	15.72

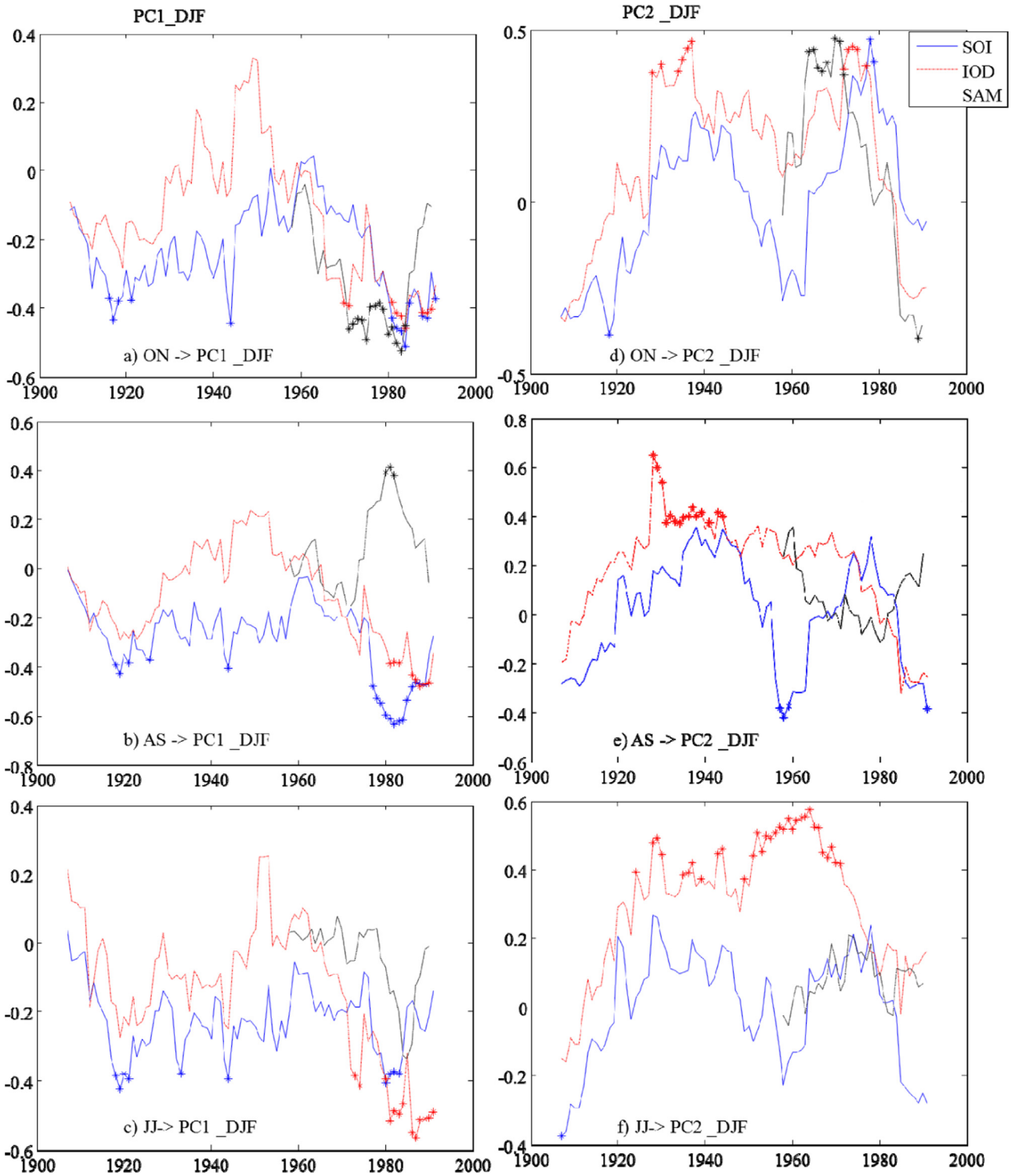

Fig. 5. Running correlation coefficients for the first two PCs of summer rainfall with the lagged climatic indices. (a) Shows the running correlations of summer PC1 with SOI_{ON}, IOD_{ON} and SAM_{ON}. (b) Shows running correlations of PC1 with SOI_{AS}, IOD_{AS} and SAM_{AS}. (c) Shows running correlations of PC1 with SOI_{JJ}, IOD_{JJ} and SAM_{JJ}. Figure e, f, g shows PC2 running correlation with the same lags of climate indices as a, b and c, respectively. The correlation is calculated over 21-year windows. The '*' indicates statistically significant correlation (P-value < 0.05).

Generally, summer predictors from IOD and SOI are correlated; IOD and SOI over Oct–Nov and Aug–Sep showed continuous significant positive correlations (Table 4). The average of SOI and IOD over Jun–July displayed a higher correlation value from 1907 up to 1957, which subsequently becomes insignificant after 1958 and up to recent decades. On the other hand, the effect of IOD_{JJ} on both PC1 and 2 in summer is strong (Fig. 5c and f). SAM indices have no correlation with both IOD and SOI (Table 4).

Summer anomalies are correlated positively and negatively with PC1 and PC2 respectively (Fig. 3(a, b), and Table 2). The PC1 and PC2 of summer rainfall were negatively and positively correlated with IOD from the beginning of the 1970s up to recent decades, if IOD is lagged by up to 6 months, i. e. IOD_{ON} (Fig. 5a), IOD_{AS} (Fig. 5b) and IOD_{JJ} (Fig. 5c). This demonstrates that summer

Table 4
Correlation between climate index predictors used of each season, significant correlations ($P <= 0.05$) marked by "*".

			1907–2011			1907–1957			1958–2011		
			SOI	IOD	SAM	SOI	IOD	SAM	SOI	IOD	SAM
Summer predictors	Oct–Nov	SOI									
		IOD	0.52*			0.46*			0.56*		
		SAM							0.08	0.12	
	Aug–Sep	SOI									
		IOD	0.46*			0.52*			0.41*		
		SAM							−0.1	−0.006	
	Jun–July	SOI									
		IOD	0.28*			0.43*			0.2		
		SAM							−0.14	−0.12	
Autumn-predictor	Jan–Feb	SOI									
		IOD	−0.2*			−0.06			−0.3*		
		SAM							0.14	−0.35*	
	Nov–Dec	SOI									
		IOD	0.26*			0.17			0.28*		
		SAM							0.35*	0.097	
	Sep–Oct	SOI									
		IOD	0.57*			0.5*			0.6*		
		SAM							−0.13	0.032	
Winter predictors	Apr–May	SOI									
		IOD	0.08			−0.02			0.18		
		SAM							0.0076	0.099	
	Feb–Mar	SOI									
		IOD	−0.2*			0.002			−0.38*		
		SAM							0.16	−0.32*	
	Dec–Jan	SOI									
		IOD	0.18*			0.1*			−0.27*		
		SAM							0.2 (0.1)	−0.23 (0.1)	
Spring-predictors	Jul–Aug	SOI									
		IOD	0.39*			0.48*			0.33*		
		SAM							−0.2 (0.1)	−0.63*	
	May–Jun	SOI									
		IOD	0.26*			0.3*			0.12		
		SAM							−0.04	−0.04	
	Mar–Apr	SOI									
		IOD				−0.03			−0.27*		
		SAM	0.14 (0.1)						0.2	−0.23 (0.1)	

rainfall variations are negatively correlated with IOD indices. An exception was an insignificant period from 1973 to 1980 (Fig. 5b). Consequently, the IOD displays higher negative correlations for summer rainfall in the south-eastern and eastern region of Australia from 1980.

Positive scores of PC1 are strongly correlated (r=0.85) to positive rainfall anomalies, or wet years, (Fig. 3(a, b), and Table 2). The running correlations between $PC1_{DJF}$ with SOI are negative and significant in some, but not all decades (e. g. 1920s, 1930s, 1950s, 1980s, 1990s and 2000s). The negative correlation of SOI with summer PC1 corresponds to the strongest El Nino events such as 1982–1983, and 1997–1998 (Meyers et al., 2007). Higher negative correlations between SOI with $PC1_{DJF}$ occurred during recent decades. Running correlations yield similar results for different lags of SOI and IOD with $PC1_{DJF}$, but correlations between $PC1_{DJF}$ and lagged IOD are more significant than those with SOI. This confirms that there is a stronger recent effect of IOD in comparison to SOI on Australian rainfall variability, as observed by Cai et al. (2013), at least for the summer.

The correlations between SAM_{AS} and SAM_{JJ} with $PC1_{DJF}$ are non-significant (Fig. 5b and c). Although SAM_{ON}, similar to IOD_{ON} and SOI_{ON}, displays negative correlations with $PC1_{DJF}$ (Fig. 5a), there is a clear change in correlation coefficients between SAM_{ON} with $PC1_{DJF}$ during 1970–1990 (for a 20-years window) where the relationship becomes significantly negative (Fig. 5a).

The results of the analysis related to the summer PC1 confirms

that rainfall anomalies during recent decades have much stronger negative correlations with the lagged signals of three indices SAM, IOD and SOI. That was expected for SAM and IOD but not necessarily for SOI; it may be due to the stronger effect of other indices in summer time and the effect of ENSO on air temperature (Ummenhofer et al., 2009). The average IOD over Jun–July (Fig. 5 -c), SOI over Oct–Nov and Aug–Sep (Fig. 5a, b), and SAM over Oct–Nov (Fig. 5a) demonstrate a stronger correlation with summer rainfall variations. The effect of average IOD over Jun–July on summer rainfall is stronger followed by change in link between IOD_{JJ} and SOI_{JJ} over 1958–2011 (Table 4).

The positive scores of PC2 are correlated negatively with summer rainfall anomalies at −0.42 (dry years, Fig. 3b and Table 2). The running correlations between $PC2_{DJF}$ with the average of the leading two months climate indices (SOI_{ON}, IOD_{ON}, SAM_{ON}) are shown in Fig. 5. The correlations between $PC2_{DJF}$ with IOD, considering all the different lags i.e., IOD_{ON}, IOD_{AS} and IOD_{JJ} (Fig. 5a, b, c), are positive (significant points). The strength of IOD

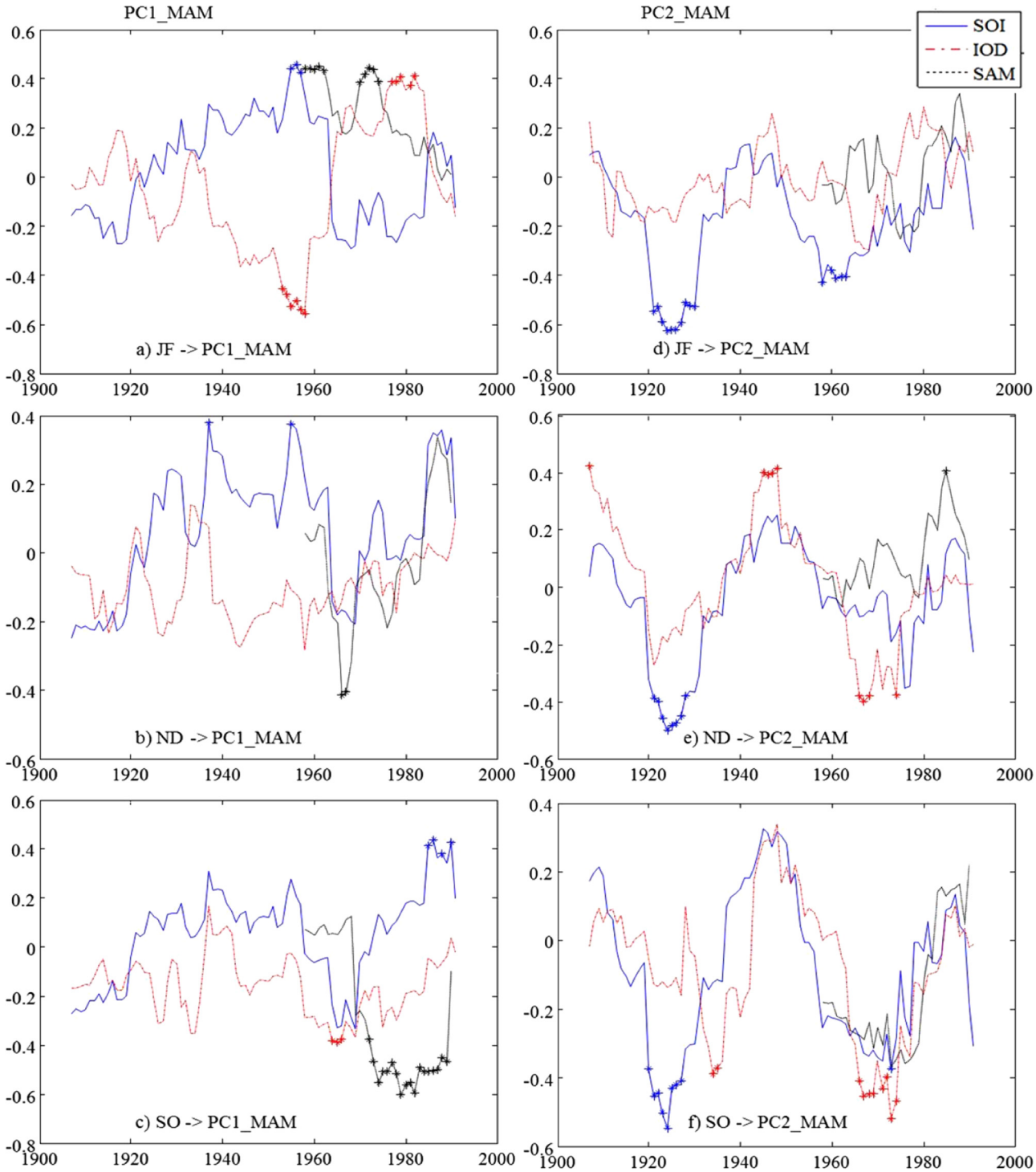

Fig. 6. Running correlation coefficients for the first two PCs of autumn rainfall with the lagged climatic indices. (a) shows the running correlation of PC1 and IOD_{JF}, SOI_{JF} and SAM_{JF}. (b) shows running correlation of PC1 and IOD_{ND}, SOI_{ND} and SAM_{ND}. (c) shows running correlation of PC1 and IOD_{SO}, SOI_{SO} and SAM_{SO}. (e, f, g) Shows the PC2 running correlation with the same lag climate indices as a, b and c, respectively. The correlation is calculated over 21-year windows. The '*' indicates statistically significant correlation (P-value < 0.05).

relationships with $PC2_{DJF}$ changed, depending on the lag. The correlations between $PC2_{DJF}$ and IOD are significant for most of the period up to 1970. The sign of the loadings of the summer PCs (Fig. 5a, b) is important when interpreting the effect of climate indices. For example, IOD has a negative correlation with anomalies of the summer rainfall in the area. The effect of IOD on the variations, explained by $PC1_{DJF}$, is similar across the entire area, reflecting the positive loadings for the entire area. In the case of the $PC2_{DJF}$, with a bipolar spatial pattern and negative correlation with IOD, higher IOD leads to decreasing rainfall in the area with positive loadings and increasing rainfall in the area with negative loading. Therefore, from the result of $PC2_{DJF}$, a higher IOD leads to more rainfall in summer in the central and southern areas and less rainfall in the coastal area.

The correlations between SAM and $PC2_{DJF}$ were positive during the 1970s (considering a 20-year window). In addition, significant correlations occurred between $PC2_{DJF}$, both negative and positive, in some decades with lagged SOI. Overall, the correlation of SOI with PC2 of summer does not appear to be stable.

The results of the running correlations of climate indices with summer rainfall PCs demonstrate the negative correlations of these indices with summer rainfall anomalies (not considering some positive correlations of SOI_{AS} and SAM_{ON} with PC2). Different lags of IOD and SOI with summer PCs show similar correlations. Both PCs of the summer have significant correlations with IOD over June–July (especially with the average of six and five months lag) (Fig. 5c, and e). In recent decades, after 1970, there was a stronger impact of IOD on $PC1_{DJF}$, which is related to a higher variation of summer rainfall. These higher correlations of summer PCs with IOD_{JJ} during recent decades indicate the important effect of this lag of IOD on summer rainfall (Fig. 5c). The correlations between climate indices used to study the cause of the variation in summer rainfall are provided in Table 4. There is strong significant correlation between SOI indices and corresponding IOD indices used for summer. Similar relationships of SOI and IOD indices with summer rainfall can be due to high interaction between these indices during this season (Table 4).

3.2.2. Autumn

For the climate indices in autumn, the average value of the last two months from the start of the season, Jan–Feb, was denoted as SOI_{JF}, IOD_{JF} and SAM_{JF} (Fig. 6a and d); the average value of the three and four months, Nov–Dec, denoted as SOI_{ND}, IOD_{ND} and SAM_{ND} (Fig. 6b and e); and the average value of the last five and six months, Sep–Oct, denoted as SOI_{SO}, IOD_{SO} and SAM_{SO} (Fig. 6c and f).

$PC1_{MAM}$ shows statistically significant positive correlation with SOI in some decades (Fig. 6a). The average SOI over Sep–October, SOI_{SO}, displays stronger positive correlations with $PC1_{MAM}$ during recent decades. For IOD, especially IOD_{JF}, the sign of correlations with $PC1_{MAM}$ changed during different decades. The significant negative correlations of the $PC1_{MAM}$ with IOD during 1950–1960 (considering a 20 year window) changed to positive (with IOD_{JF}) since 1970 (Fig. 6 a, b and c). This may be due to change in the interaction between IOD_{JF} and SOI_{JF} (Table 4 – autumn predictors). The most significant correlations between SAM with $PC1_{MAM}$ happened with the average SAM during September–October (Fig. 6c). The impact of SAM on the autumn rainfall anomalies variations, $PC1_{MAM}$, indicates different types of correlations, varying from positive to negative after 1970 (Fig. 6a, b and c).

SOI_{JF} and IOD_{JF} are negatively linked; this significant negative correlation was stronger (-0.3) during 1958–2010 (Table 4). As a result, reverse patterns of correlation between autumn PCs with SOI_{JF} and IOD_{JF} are due to the negative correlation (Fig. 6(a)-d and Table 4). In comparison, the correlation between SOI_{ND}/SOI_{SO} with IOD_{ND}/IOD_{SO} (Table 4-autumn predictors) was positive; they represent similar correlations with both PCs of autumn, with stronger correlations with SOI_{SO} during the recent decades. SAM indices, as autumn predictors, demonstrated different correlations with IOD and SOI; SAM_{JF} is negatively correlated with IOD_{JF} with a value of -0.35; while, SAM_{ND} is positively correlated with SOI_{ND} with a value of 0.35 (Table 4 – autumn predictors).

The scores of $PC2_{MAM}$ had positive correlation with autumn rainfall anomalies with an overall value of 0.3; which changed from the value of 0.24 during 1907–1960 to 0.5 over 1961–2011 (Table 2). The correlations between $PC2_{MAM}$, which explained less variation than the PC1, with SOI are negative during the 1920s and 1930s, 1960s The correlations of IOD, considering all the lags, with $PC2_{MAM}$ were variable during different decades, starting from the positive correlation from 1907 to negative during the 1930s with IOD_{SO}, to positive with IOD_{ND} and IOD_{SO} during 1960–1980, followed by weak positive correlation in recent decades (Fig. 6d, e and f).

The trend of the correlation of SOI with the $PC1_{MAM}$ is strengthening, and the sign of correlations between SAM and IOD with $PC1_{MAM}$ changed in recent decades.

For the autumn PCs the results illustrate several important findings; 1) there are recent strong positive correlations of SOI over Sep–Oct with autumn rainfall; 2) the change in the correlation sign of the IOD during different decades shifts to a recent higher positive impact; 3) SAM over Sep–Oct indicates a strong impact on autumn rainfall variations; 4) IOD and SAM (especially SAM_{SO}) were more important than SOI for both of the autumn PCs. In the recent decades the SOI and IOD effect on autumn rainfall was stronger with positive correlations; in contrast SAM indicates a negative correlation with autumn rainfall anomalies; 5) correlation between autumn predictors varied by time lags. SOI and IOD over Jun–July and Aug–Sep are positively correlated; where this relationship changed to negative correlation over Jan–Feb. For SAM indices, IOD and SAM is correlated with IOD over Jan–Feb negatively and SOI over Aug–Sep positively.

3.2.3. Winter

Similar to the earlier analysis, running correlations for the first two PCs of winter (JJA) rainfall versus climate indices for up to six months were calculated: The average of climate indices over, Apr–May, SOI_{AM}, IOD_{AM} and SAM_{AM} (Fig. 7a and d); the average for Feb–Mar, SOI_{FM}, IOD_{FM} and SAM_{FM} (Fig. 7b and e); and the average of Dec–Jan, SOI_{DJ}, IOD_{DJ} and SAM_{DJ} (Fig. 7c and f).

The winter PC1 corresponds to positive anomalies of winter rainfall (Fig. 3e and Table 2), but less strongly than for summer and autumn, while winter PC2 shows stronger correlation with winter anomalies.

Table 4 (winter predictors) shows the correlations between predictors of winter rainfall considered in the current study. SOI, IOD and SAM over Apr–May had no significant correlations; the correlation between IOD_{FM} with SOI_{FM} is not significant up to 1958, but this correlation changes to negative after 1958. During Dec–Jan, SOI and IOD have a weak positive correlation shifting to a statistically significant negative with a value of -0.32 from 1958. Understanding the change in the correlation between IOD and SOI might help clarify climate variations in the area.

SOI shows decreasing positive correlations with PCI_{JJA}. The exception on this is a negative correlation between $PC1_{JJA}$ and SOI_{AM} during 1910–1920 (Fig. 7a). Longer lag times of SOI weaken the relationship with $PC1_{JJA}$ (Fig. 7a, b and c). The decreasing correlations of IOD and SOI with $PC1_{JJA}$, during Feb–Mar, and Dec–Jan, started around 1950 (Fig. 7b and c). This change is corresponding to the change of the links between these indices of IOD and SOI after 1958 (Table 4 – winter predictors). Both IOD and SOI started the century with positive correlations with winter rainfall anomalies and changed to negative or insignificant correlations.

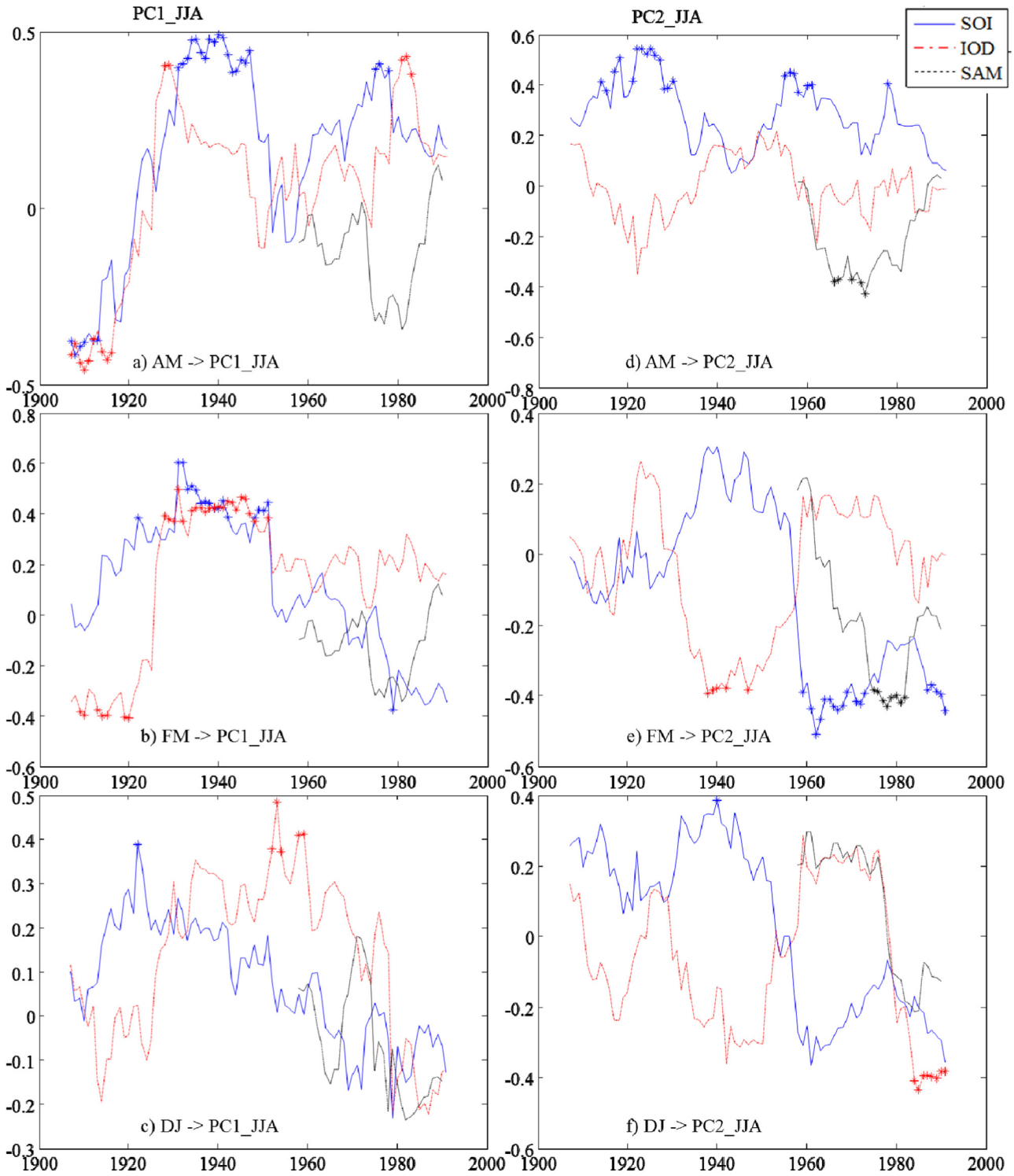

Fig. 7. Running correlation coefficients for the first two PCs of winter rainfall with the lagged climatic indices. (a) Shows running correlation of PC1 and IOD $_{AM}$, SOI_{AM} and SAM_{AM}. (b) Shows running correlation of PC1 and IOD $_{FM}$, SOI_{FM} and SAM_{FM}. (c) Shows running correlation of PC1 and IOD_{DJ}, SOI_{DJ} and SAM_{DJ}. (e, f, g) Shows the PC2 running correlation with the same lag climate indices as a, b and c, respectively. The correlation calculated over 21-year windows. The '*' indicates statistically significant correlation (P-value < 0.05)

$PC1_{JJA}$ did not show strong correlations with climate indices after 1960 s (Fig. 7a, b and c). All SAM predictors had insignificant correlations with $PC1_{JJA}$ (Fig. 7a, b and c).

Running correlations between $PC2_{JJA}$ and SOI_{AM} are positive but decreasing over time. The most significant link between $PC2_{JJA}$ and climate indices is the increasing negative correlations with SOI_{FM} since 1958 (Fig. 7e). Correlations between $PC2_{JJA}$ with SOI_{FM} and SOI_{DJ} follow similar trends (Fig. 7d, e and f). Higher SOI over Feb–Mar reduce winter rainfall, mainly in the areas with a winter rainfall regime (given the loadings sign Fig. 4). SAM and IOD gave negative correlations with $PC2_{JJA}$. Significant changes in correlations between IOD_{DJ} and $PC2_{JJA}$ during 1982–2010 can be observed (Fig. 7f). Similarly, the positive IOD during Dec–Jan indicates less rainfall in winter. Greater and more significant correlations

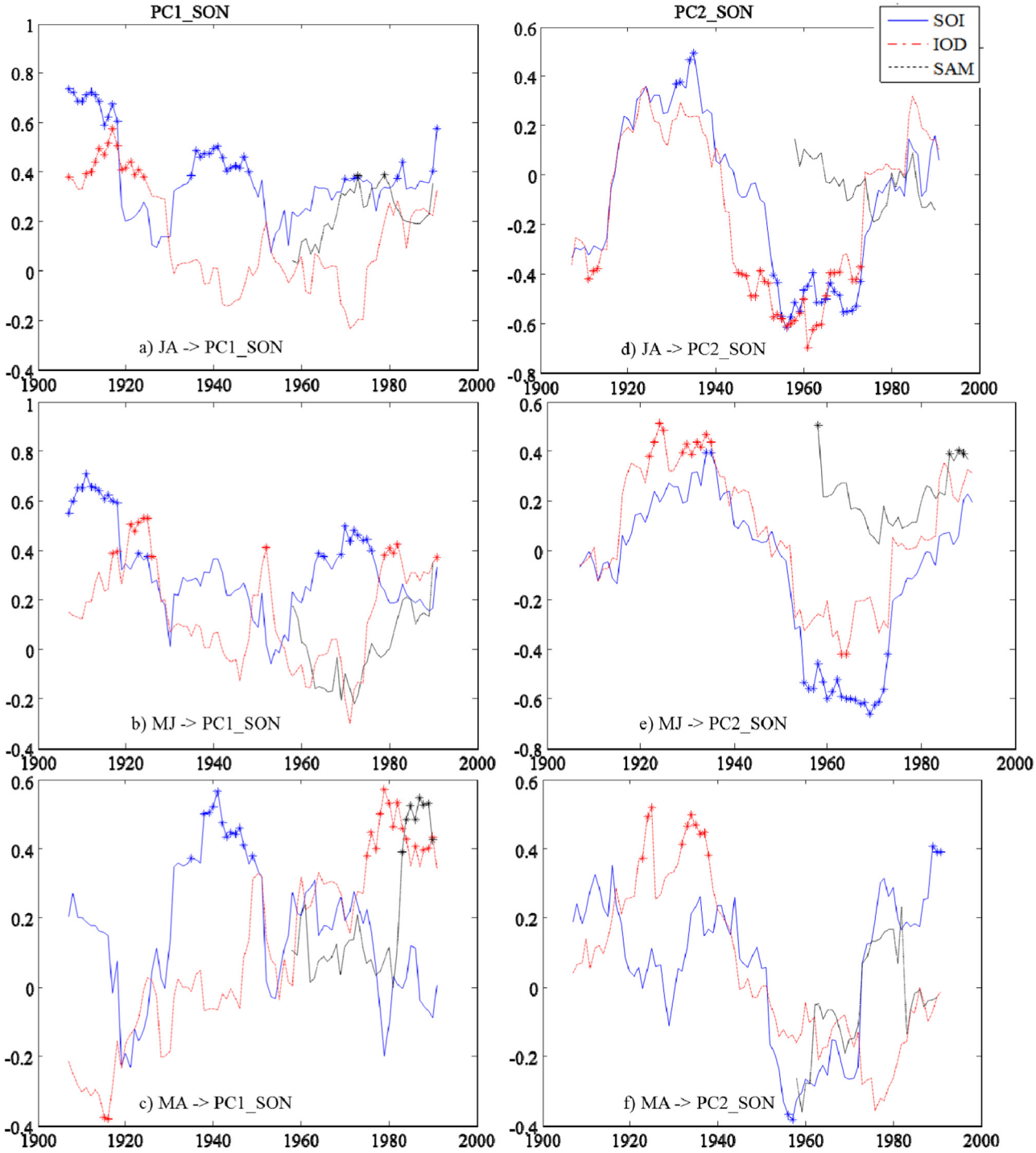

Fig. 8. Running correlation coefficients for the first two PCs of spring rainfall with the lagged climatic indices. (a) Shows running correlation of the PC1 winter and IOD_{JA}, SOI_{JA} and SAM_{JA} (b) shows running correlations of the PC1 winter and IOD_{MJ}, SOI_{MJ} and SAM_{MJ}. (c) Shows running correlation of the PC1 of the winter and IOD_{MA}, SOI_{MA} and SAM_{MA}. (e, f, and g) Show the PC2 running correlation with the same lag of climate indices as a, b and c. The correlation calculated over 21-year windows. The '*' indicates statistically significant correlation (P-value < 0.05).

between SAM and $PC2_{JJA}$ occur after 1970 but disappear around 1980. The running correlations between SAM_{AM} and SAM_{FM} with $PC2_{JJA}$ are negative during 1970–1990 (Fig. 7d and e).

In winter, the results demonstrated several important findings; 1) the correlation between IOD and SOI indices, considered for winter, changed from 1958 (Table 4 – winter predictors); 2) The average of IOD and SOI over five and six month before the start of season, Dec–Jan, shows a recent stronger negative impact on winter rainfall; 3) the correlation of SOI_{FM} and SOI_{DJ} with winter rainfall changed after 1958 from positive to negative; 4) SAM shows a strong negative correlation with winter rainfall variations. The strength of SAM indices correlations with winter rainfall varies from decade to decade for each SAM indices (Table 4 – winter predictors).

3.2.4. Spring

Finally for spring, lagged climate indices for up to six months: two months, are SOI_{JA}, IOD_{JA} and SAM_{JA} (Fig. 8a and d); three to four months, are SOI_{MJ}, IOD_{MJ} and SAM_{MJ} (Fig. 8b and e); and five

and six months are SOI_{MA}, IOD_{MA} and SAM_{MA} (Fig. 8c and f).

$PC1_{SON}$ is highly correlated with the spring rainfall anomalies (Table 4). The correlations between IOD and SOI with $PC1_{SON}$ and spring rainfall anomalies are positive and stronger during July–Aug compared to other lagged predictors of these indices (Fig. 8a). The strength of the correlations between SOI and $PC1_{SON}$ depends on the lag of the predictors, although they follow similar trends (Fig. 8a, b and c). Similar to SOI, significant correlations between the $PC1_{SON}$ with IOD are positive apart from IOD_{MA} around 1910 (Fig. 8a, b, and c). Correlations between $PC1_{SON}$ with IOD indices tend to increase, particularly, IOD_{MA} which has positive correlations since 1980 (Fig. 8c). The correlations between IOD_{MA} and SOI_{MA} vary from insignificant to negative since 1958 (Table 4). As a result, spring rainfall variations in the recent decades have higher positive correlations with IOD_{MA} and SAM_{MA}. The strongest effect of SAM_{MA} occurs since 1983 (Fig. 8c).

Higher negative correlations of $PC2_{SON}$ with SOI and IOD occur during 1940–1970 (considering a 20 years window) (Fig. 8-d, e and f). Thus, higher SOI and IOD lead to more rainfall in the coastal area (positive loadings) and less rainfall in winter rainfall regime areas (negative loadings). The effects of SOI and IOD on the $PC2_{SON}$ were variable from negative since 1907, to positive during 1920–1960; changing to negative from 1940 to 2000. The correlations of the $PC2_{SON}$ with IOD and SOI recently changed to positive (although not statistically significant).

In spring, the results show several important findings; 1) the average IOD and SAM of the last five and six months before, Mar–Apr, demonstrates stronger positive correlations with spring rainfall since 1970; 2) stronger recent effect of SOI during July–Aug on spring rainfall; 3) large amount of variation of spring rainfall (PC1) were positively correlated with SOI, SAM and IOD; 4) recent stronger effect of IOD and SAM than SOI on spring rainfall variations.

4. Discussion and conclusions

There are two major historical governmental seasonal forecast systems based on statistical models in Australia. These rainfall forecast systems were developed using statistical models applied to climate indices. The first forecast system is run by Queensland government (QG) and is ENSO-based using SOI-phases (Stone and Auliciems, 1992). The second forecast was run by Australian Bureau of Meteorology (BoM) and was Sea Surface Temperature (SST)-based. Sea Surface Temperatures used in the BoM forecast system extracted from both the Indian and Pacific oceans regions (Drosdowsky and Chambers, 2001; Fawcett, 2008; Fawcett et al., 2005). Fawcett and Stone (2010) compared the performance of the two governmental forecasting systems developing a hindcast for 1997–2009. The comparison of the result of hindcast of two available forecast systems indicates that BoM's system produced more reliable results than the reconstructed SOI-phases based forecasting system run by QG. The main issue with statistical models is that they rely on stationary relationships between the predictors and predictand variables, and climate change can change these relationships (Schepen et al., 2012).

Currently the Australian Bureau of Meteorology (BoM) developed a dynamical seasonal prediction system based on a Predictive Ocean Atmosphere Model (POAMA) for Australia. This system is a coupled ocean-atmosphere climate model and data assimilation system (Alves et al., 2003; Hudson et al., 2011; Lim et al., 2010; Lim et al., 2009b; Zhao and Hendon, 2009). The main advantage of POAMA model as a general circulation model (GCM) is their ability to capture nonlinear interactions between atmosphere, land and ocean, and its adaptation to shifts in climate as a physical based model (Schepen et al., 2012). However, GCMs suffer from being overconfident and normally their simulations are not aligned with corresponding observations (Graham et al., 2005; Lim et al., 2009a). Therefore, statistical models are used to calibrate raw GCM output to obtain statistically reliable forecasts and closer prediction to observed data (Landman and Goddard, 2002). A hybrid forecast system using strengths of statistical model based on lagged climatic indices and dynamical modelling approaches (POAMA) improves Australian seasonal rainfall forecasting system (Schepen et al., 2012). Therefore, improvement in statistical models can still lead in a significant improvement in regional climate forecasting. Understanding the mechanism responsible for rainfall variability in relation to climatic indices and stability of temporal and spatial relationship between these climatic indices with rainfall variability is desirable before developing any credible statistical climate forecasting scheme, despite the advances in numerical climate forecasting.

Recent change in strength and frequency of IOD events affects Australian climate (Cai et al., 2012). In addition, there are limitations of the predictability of the Australian rainfall using major climate indices as they can address a limited amount of the rainfall variation (Westra and Sharma, 2010).

In the current study we analysed the long-term seasonal rainfall variability over south-eastern and eastern Australia using an updated high quality dataset from Australian BoM. The main variations of rainfall in south-eastern and eastern Australia were clearly season-dependent.

The results of running linear correlations between seasonal rainfall and lagged climatic indices indicated that the strength of the correlation between lagged SAM, SOI and IOD over south-eastern and eastern Australia and interaction between these climate indices are highly season-dependent. As in some season different lags are stronger or even the correlation direction is changing, appropriate lag selection is important issue for seasonal rainfall forecasting. Also, the sign and strength of the correlation with climatic indices for each season were different. These findings provide reasonable evidence to discontinue using fixed variables as predictors of all seasons in the area.

Stronger recent, approximately after 1970, correlations with these three indices especially with IOD are evident. The recent strong correlation could be consistent with expected consequences of global warming (Cai et al., 2013; Zhong et al., 2005). Cai et al. (2013) investigated the projected response of the IOD to greenhouse warming. Their results also indicated that the effects of IOD on Australian rainfall are getting stronger.

The interactions between SOI and IOD varies with both inter-annually and on decadal scales. Significant amount of recent climate variability can be due to the change of the interaction between SOI and IOD which will need further investigation.

One of the results of this study is that the relationship between climate indices (SOI, SAM and IOD) with seasonal rainfall changes during different decades. Understanding of the links and physical mechanism explaining these links will increase the ability to develop better seasonal prediction systems. There are some periodic patterns of SOI and IOD within these non-stationary relationships. Regrettably, the period of available observational data is still not enough to reveal the cause and effect of these relationships. Further study will be needed to clarify and investigate the mechanism of change in the effect of IOD on rainfall variability over south-eastern and eastern Australia. This can be clarified by investigating the equality and similarity of the effect of climate change on SST of both Indian and Pacific oceans. Pacific and Indian oceans events can also result in a change of temperature (Meyers et al., 2007). Therefore, a relationship between temperature variations (due to both climate change and variability caused by ocean events) together with variations of climatic indices with seasonal rainfall will need to be analysed much more systematically.

This study aims to identify the effect of the Indian, pacific and Antarctic Oceans on South-eastern and east Australian seasonal rainfall and their long-term interactions. As a result, SAM, IOD and SOI which are demonstrating the oscillation of these oceans are selected to simplify the analysis. Additional investigation of the potential effect of NINO3, NINO4, NINO1, NINO2 and the Inter-decadal Pacific Oscillation (IPO) on long term rainfall variability in south-eastern and East Australian rainfall would be beneficial.

The analysis for SAM is limited to 1957 as in the current study we used Marshal Index. The analysis using other calculations of SAM index with longer periods of availability, i. e., Visbeck Index can be beneficial (Ho et al., 2012).

References

Alves, O., et al., 2003. POAMA: bureau of Meteorology operational coupled model seasonal forecast system. In: Proceedings of National Drought Forum, Brisbane, pp. 49–56.

Ashok, K., Guan, Z.Y., Yamagata, T., 2003. A look at the relationship between the ENSO and the Indian Ocean Dipole. J. Meteorol. Soc. Jpn. 81 (1), 41–56.

Cai, W., Cowan, T., Sullivan, A., 2009. Recent unprecedented skewness towards positive Indian Ocean Dipole occurrences and its impact on Australian rainfall. Geophys. Res. Lett. 36 (11), L11705.

Cai, W., van Rensch, P., Cowan, T., Hendon, H.H., 2012. An asymmetry in the IOD and ENSO teleconnection pathway and its impact on australian climate. J. Clim. 25 (18), 6318–6329.

Cai, W., et al., 2013. Projected response of the Indian Ocean Dipole to greenhouse warming. Nat. Geosci. 6 (12), 999–1007.

Dezfuli, A.K., 2011. Spatio-temporal variability of seasonal rainfall in western equatorial Africa. Theor. Appl. Climatol. 104 (1–2), 57–69.

Drosdowsky, W., 1993. An analysis of Australian seasonal rainfall anomalies 1950–1987: spatial patterns. Int. J. Climatol. 13 (1), 1–30.

Drosdowsky, W., 2002. SST phases and Australian rainfall. Aust. Meteorol. Mag. 51 (1), 1–12.

Drosdowsky, W., Chambers, L.E., 2001. Near-global sea surface temperature anomalies as predictors of Australian seasonal rainfall. J. Clim. 14 (7), 1677–1687.

Evans, A.D., Bennett, J.M., Ewenz, C.M., 2009. South Australian rainfall variability and climate extremes. Clim. Dyn. 33 (4), 477–493.

Evans, J.L., Allan, R.J., 1992. El Nino southern oscillation modification to the structure of the monsoon and tropical cyclone activity in the Australian region. Int. J. Climatol. 12 (6), 611–623.

Fawcett, R., 2008. Verification techniques and simple theoretical forecast models. Weather Forecast. 23 (6), 1049–1068.

Fawcett, R.J.B., Jones, D.A., Beard, G.S., 2005. A verification of publicly issued seasonal forecasts issued by the Australian Bureau of Meteorology: 1998–2003. Aust. Meteorol. Mag. 54 (1), 1–13.

Fawcett, R.J.B., Stone, R.C., 2010. A comparison of two seasonal rainfall forecasting systems for Australia. Aust. Meteorol. Oceanogr. J. 60 (1), 15–23.

Gergis, J., et al., 2012. On the long-term context of the 1997–2009 'big dry' in south-eastern Australia: insights from a 206-year multi-proxy rainfall reconstruction. Clim. Change 111 (3–4), 923–944.

Graham, R.J., et al., 2005. A performance comparison of coupled and uncoupled versions of the met office seasonal prediction general circulation model. Tellus Ser. A: Dyn. Meteorol. Oceangr. 57 (3), 320–339.

Hammer, G.L., et al., 2001. Advances in application of climate prediction in agriculture. Agric. Syst. 70 (2–3), 515–553.

Hendon, H.H., Thompson, D.W.J., Wheeler, M.C., 2007. Australian rainfall and surface temperature variations associated with the southern hemisphere annular mode. J. Clim. 20 (11), 2452–2467.

Ho, M., Kiem, A.S., Verdon-Kidd, D.C., 2012. The southern annular mode: a comparison of indices. Hydrol. Earth Syst. Sci. *16* (3), 967–982.

Hudson, D., Alves, O., Hendon, H.H., Marshall, A.G., 2011. Bridging the gap between weather and seasonal forecasting: intraseasonal forecasting for Australia. Q. J. R. Meteorol. Soc. 137 (656), 673–689.

Kiem, A.S., Franks, S.W., 2004. Multi-decadal variability of drought risk, eastern Australia. Hydrol. Process. 18 (11), 2039–2050.

Kiem, A.S., Franks, S.W., Kuczera, G., 2003. Multi-decadal variability of flood risk. Geophys. Res. Lett. 30 (2). http://dx.doi.org/10.1029/2002GL015992.

Kirono, D.G.C., Chiew, F.H.S., Kent, D.M., 2010. Identification of best predictors for forecasting seasonal rainfall and runoff in Australia. Hydrol. Process. 24 (10), 1237–1247.

Landman, W.A., Goddard, L., 2002. Statistical recalibration of GCM forecasts over southern Africa using model output statistics. J. Clim. 15 (15), 2038–2055.

Lavery, B., et al., 1997. An extended high-quality historical rainfall dataset for Australia. Aust. Meteorol. Mag. 46 (1), 27–38.

Lim, E.-P., Hendon, H.H., Anderson, D.L.T., Charles, A., Alves, O., 2010. Dynamical, statistical–dynamical, and multimodel ensemble forecasts of australian spring season rainfall. Mon. Weather Rev. 139 (3), 958–975.

Lim, E.-P., Hendon, H.H., Hudson, D., Wang, G., Alves, O., 2009a. Dynamical forecast of inter-El nino variations of tropical SST and Australian spring rainfall. Mon. Weather Rev. 137 (11), 3796–3810.

Lim, E.P., Hendon, H.H., Hudson, D., Wang, G.M., Alves, O., 2009b. Dynamical forecast of inter-El nino variations of tropical SST and Australian spring rainfall. Mon. Weather Rev. 137 (11), 3796–3810.

Marshall, G.J., 2003. Trends in the southern annular mode from observations and reanalyses. J. Clim. 16 (24), 4134–4143.

Meyers, G., McIntosh, P., Pigot, L., Pook, M., 2007. The years of El Nino, La Nina, and interactions with the tropical Indian ocean. J. Clim. 20 (13), 2872–2880.

Murphy, B.F., Timbal, B., 2008. A review of recent climate variability and climate change in southeastern Australia. Int. J. Climatol. 28 (7), 859–879.

Nelson, R., et al., 2010. The vulnerability of Australian rural communities to climate variability and change: Part II—integrating impacts with adaptive capacity. Environ. Sci. Policy 13 (1), 18–27.

Nicholls, N., 1989. Sea surface temperatures and Australian winter rainfall. J. Clim. 2 (9), 965–973.

Nicholls, N., 2010. Local and remote causes of the southern Australian autumn-winter rainfall decline, 1958–2007. Clim. Dyn. 34 (6), 835–845.

Richman, M.B., 1986. Rotation of principal components. J. Climatol. 6 (3), 293–335.

Risbey, J.S., Pook, M.J., McIntosh, P.C., Wheeler, M.C., Hendon, H.H., 2009. On the remote drivers of rainfall variability in Australia. Mon. Weather Rev. 137 (10), 3233–3253.

Robertson, D.E., Pokhrel, P., Wang, Q.J., 2013. Improving statistical forecasts of seasonal streamflows using hydrological model output. Hydrol. Earth Syst. Sci. 17 (2), 579–593.

Saji, N.H., Goswami, B.N., Vinayachandran, P.N., Yamagata, T., 1999. A dipole mode in the tropical Indian ocean. Nature 401 (6751), 360–363.

Schepen, A., Wang, Q.J., Robertson, D.E., 2012. Combining the strengths of statistical and dynamical modeling approaches for forecasting Australian seasonal rainfall. J. Geophys. Res. – Atmos., 117.

Smith, T.M., Reynolds, R.W., Peterson, T.C., Lawrimore, J., 2008. Improvements to NOAA's historical merged land-ocean surface temperature analysis (1880–2006). J. Clim. 21 (10), 2283–2296.

Stone, R., Auliciems, A., 1992. SOI phase relationships with rainfall in eastern Australia. Int. J. Climatol. 12 (6), 625–636.

Stone, R.C., Hammer, G.L., Marcussen, T., 1996. Prediction of global rainfall probabilities using phases of the southern oscillation index. Nature 384 (6606), 252–255.

Troup, A.J., 1965. Southern oscillation. Q. J. R. Meteorol. Soc. 91 (390) 490.

Ummenhofer, C.C., et al., 2009. What causes southeast Australia's worst droughts? Geophys. Res. Lett. 36. http://dx.doi.org/10.1029/2008GL036801.

Verdon, D.C., Franks, S.W., 2005a. Indian ocean sea surface temperature variability and winter rainfall: eastern Australia. Water Resour. Res. 41, 9.

Verdon, D.C., Franks, S.W., 2005b. Influence of Indian ocean sea-surface temperature variability on winter rainfall across eastern Australia. In: Wagener, T., et al. (Eds.), Regional Hydrological Impacts of Climatic Change – Impact Assessment and Decision Making. Iahs Publication, pp. 335–345.

Verdon, D.C., Franks, S.W., 2006. Long-term behaviour of ENSO: interactions with the PDO over the past 400 years inferred from paleoclimate records. Geophys. Res. Lett 33, 6, http://dx.doi.org/10.1029/2005GL025052.

Verdon, D.C., Wyatt, A.M., Kiem, A.S., Franks, S.W., 2004. Multidecadal variability of rainfall and streamflow: eastern Australia. Water Resour. Res. 40 (10), W10201.

Wang, G., Hendon, H.H., 2007. Sensitivity of Australian rainfall to inter-El Nino variations. J. Clim. 20 (16), 4211–4226.

Westra, S., Sharma, A., 2010. An upper limit to seasonal rainfall predictability? J. Clim. 23 (12), 3332–3351.

Wheeler, M.C., Hendon, H.H., 2004. An all-season real-time multivariate MJO index: development of an index for monitoring and prediction. Mon. Weather Rev. 132 (8), 1917–1932.

Wheeler, M.C., Hendon, H.H., Cleland, S., Meinke, H., Donald, A., 2009. Impacts of the Madden–Julian oscillation on Australian rainfall and circulation. J. Clim. 22 (6), 1482–1498.

Zhao, M., Hendon, H.H., 2009. Representation and prediction of the Indian Ocean dipole in the POAMA seasonal forecast model. Q. J. R. Meteorol. Soc. 135 (639), 337–352.

Zhong, A.H., Hendon, H.H., Alves, O., 2005. Indian ocean variability and its association with ENSO in a global coupled model. J. Clim. 18 (17), 3634–3649.

Zveryaev, I., 2006. Seasonally varying modes in long-term variability of European precipitation during the 20th century. J. Geophys. Res. 111. http://dx.doi.org/10.1029/2005JD006821.